

RSC Advances



This is an *Accepted Manuscript*, which has been through the Royal Society of Chemistry peer review process and has been accepted for publication.

Accepted Manuscripts are published online shortly after acceptance, before technical editing, formatting and proof reading. Using this free service, authors can make their results available to the community, in citable form, before we publish the edited article. This *Accepted Manuscript* will be replaced by the edited, formatted and paginated article as soon as this is available.

You can find more information about *Accepted Manuscripts* in the [Information for Authors](#).

Please note that technical editing may introduce minor changes to the text and/or graphics, which may alter content. The journal's standard [Terms & Conditions](#) and the [Ethical guidelines](#) still apply. In no event shall the Royal Society of Chemistry be held responsible for any errors or omissions in this *Accepted Manuscript* or any consequences arising from the use of any information it contains.

Magnetic Mesoporous Silica Nanoparticles for CpG Delivery to Enhance Cytokine Induction via Toll-like Receptor 9

Cuilian Tao^a, Yufang Zhu^{b*}, Xianglan Li^c, Nobutaka Hanagata^c

^a School of Medical Instrument and Food Engineering, University of Shanghai for Science and Technology, 516 Jungong Road, Shanghai, 200093, China.

^b School of Materials Science and Engineering, University of Shanghai for Science and Technology, 516 Jungong Road, Shanghai, 200093, China.

^c Nanotechnology Innovation Station, National Institute for Materials Science, 1-2-1 Segen, Tsukuba, Ibaraki 305-0047, Japan.

*Corresponding authors: Yufang Zhu

Tel: +86-21-55271663;

Email: zjf2412@163.com

Abstract : We developed a potential cytosine-phosphate-guanosine oligodeoxynucleotides (CpG ODN) delivery system based on magnetic mesoporous silica (MMS) nanoparticles by binding of CpG ODN onto aminated MMS (MMS-NH₂) nanoparticles to form CpG/MMS-NH₂ complexes for Toll-like receptor 9 (TLR9)-mediated induction of cytokines. Magnetization, serum stability, in vitro cytotoxicity, cellular uptake, and interleukin-6 (IL-6) induction of CpG/MMS-NH₂ complexes were evaluated. The results showed that MMS nanoparticles exhibited superparamagnetic behavior with a saturation magnetization of 6.5 emu/g. Also, MMS-NH₂ nanoparticles had no cytotoxicity to Raw 264.7 cells, and CpG/MMS-NH₂ complexes enhanced serum stability of CpG ODN and could be localized in the endolysosomes after endocytosis by cells. Importantly, CpG/MMS-NH₂ complexes significantly enhanced the TLR9-mediated IL-6 induction compared to free CpG ODN. Therefore, CpG/MMS-NH₂ complexes could be magnetic targeted delivery and significantly enhance the TLR9-mediated cytokine induction for stimulating immune responses.

Keywords: Magnetic nanoparticles, Mesoporous silica, CpG oligodeoxynucleotides, Delivery, Toll-like receptor 9, Interleukin-6

1. Introduction

Gene therapy has been regarded as an important and promising strategy for the treatment of genetic diseases [1-3]. However, successful gene therapy is strongly dependent on the delivery carriers that deliver genes into cells for the stimulation of immune response. Generally, it is desirable for gene delivery carriers to have the capabilities of low cytotoxicity, high gene loading, efficient gene protection, cell targeting, efficient endosomal escape and controlled gene release behavior [4-5]. To date, a variety of viral and nonviral carriers (polymers, lipids, peptides, polysaccharides, inorganic species, etc.) have been developed for gene delivery, but it is still a formidable challenge to achieve satisfactory performance in gene therapy [6-7].

Recently, mesoporous silica nanoparticles (MSNs) have been a promising candidate carrier for drugs/gene delivery due to their high surface area, large pore volume, biocompatibility and ease of surface functionalization [8-10]. Recent studies also confirmed the possibility of using MSNs as a carrier for delivering nucleic acid-based drugs with high loading capacity and enhanced stability against enzymatic degradation [10-26]. For example, Du et al. developed hybridized mesoporous silica nanocarriers by linking acetaldehyde cystine modified polyethylenimine (PEI) onto amino-functionalized dendrimer-like MSNs, and hybridized nanocarriers not only showed low cytotoxicity and high gene loading capability, but also displayed high gene transfection efficiency [11]. Xia et al. reported that MSNs functionalized with 10kD PEI polymer were particularly efficient for transducing HEPA-1 cells with a

siRNA construct that was capable of knocking down GFP expression. Similarly, transfection of a GFP plasmid induced effective expression of the fluorescent protein in >70% cells in the population [12]. For most of MSNs-based gene delivery systems, MSNs carriers could be efficiently taken up by cells via endocytosis, but gene delivery efficiency mediated by MSNs carriers was strongly dependent on their endosomal escape capability [27]. Previous studies demonstrated that MSNs carriers could escape from endosomes, but the endosomal escape capability depended on the particle size and surface chemistry [27-31]. Therefore, the endosomal escape capability has been a primary factor to limit the gene delivery efficiency for most MSNs-based gene delivery systems.

CpG oligodeoxynucleotides (CpG ODN) can be used in immunotherapy for various illnesses, such as cancer, allergies/asthma, and infectious diseases [32-34]. CpG ODN can elicit the immune system through their recognition by human Toll-like receptor 9 (TLR9), a molecule located in the endolysosomes of B cells and antigen-presenting cells, and thereby mediate innate and adaptive immune response [35]. For example, TLR9 activation in B cells induces proinflammatory cytokines-including interleukin (IL)-6, IL-10 and IL-12 through nuclear factor- κ B and other signal transduction pathways, and IL-6 promotes the multiplication and activation of B cells, resulting in the enhanced production of antibodies [36-37]. Therefore, delivery systems for CpG ODN using MSNs-based carriers differ greatly from delivery systems for nucleic acid-based drugs such as antisense DNA and siRNA. For delivery of antisense DNA and siRNA using MSNs carriers, the MSNs-based

delivery system must escape from endosome to cytosol, and then the nucleic acids released from MSNs carriers transport into nucleus to induce immune response [35]. However, with the delivery of CpG ODN, CpG ODN must be retained in the endosomes/endolysosomes for a long period of time [38-43]. Because the receptor TLR9 is localized in the endosomes/endolysosomes, the CpG ODN delivery system is expected to be retained in the endosomes/endolysosomes, but not escape from endosomes.

On the other hand, magnetic property can invest unique advantages for MSNs applications with great potential for bioseparation, drug/gene delivery, and diagnostic analysis [44-49]. For example, magnetic MSNs can act as contrast agents for magnetic resonance imaging (MRI) while serving as carriers for drug/gene delivery, thus realizing simultaneous imaging and delivery [44]. Furthermore, targeted delivery is achievable because magnetic MSNs can be guided by an external magnetic field [47].

In this study, we reported a potential CpG ODN delivery system based on magnetic mesoporous silica (MMS) nanoparticles with small particle size and large mesopore size. As shown in Fig. 1, preparation of MMS nanoparticles involves the synthesis of superparamagnetic Fe_3O_4 nanoparticles and subsequently the encapsulation of Fe_3O_4 nanoparticles in mesoporous silica matrix. After modifying with amino groups on MMS nanoparticles, CpG ODN was bonded to MMS nanoparticles through the electrostatic interaction to protect against degradation by nucleases. Raw 264.7 cells were used to culture with the MMS nanoparticles-based

CpG ODN delivery system, and in vitro cytotoxicity, cellular uptake and TLR9-mediated induction of IL-6 were investigated in detail.

2. Experimental

2.1 Materials

Hexadecyltrimethylammonium p-toluenesulfonate (CTAT) and 3-aminopropyltriethoxysilane (APTES) were obtained from Sigma-Aldrich. Tetraethyl orthosilicate (TEOS), triethanolamine (TEA), ethanol, hydrochloride acid (HCl, 36-38%), potassium dihydrogen phosphate (KH_2PO_4), sodium hydroxide (NaOH), ferric chloride ($\text{FeCl}_3 \cdot 6\text{H}_2\text{O}$), ferrous chloride ($\text{FeCl}_2 \cdot 4\text{H}_2\text{O}$) were obtained from Sinopharm Chemical Reagent Co. Ltd. Agarose ITM, 6 × sucrose DNA loading buffer II, 50 × TAE buffer, ethidium bromide (EB, 10 mg/mL), fetal bovine serum (FBS), CpG ODN (72 bases), ethylenediaminetetraacetic acid disodium salt dihydrate (EDTA) were obtained from Shanghai Sangon Biotech Co. Ltd. FITC-labeled CpG ODN was purchased from FASMAC, Japan. Ultrapure water was obtained from Millipore pure water system. All chemicals were analytical-reagent grade and used without further purification.

2.2 Synthesis of magnetic mesoporous silica (MMS) nanoparticles

Magnetic Fe_3O_4 nanoparticles were synthesized according to the reported co-precipitation method [50]. Monodisperse MMS nanoparticles with uniform particle size were synthesized by using a sol-gel technique. Typically, 0.4 g of Fe_3O_4 nanoparticles was firstly dispersed in 36 ml of water under ultrasonication for 30min.

Subsequently, 0.6836 g of CTAT and 4 g of TEA were added to the Fe_3O_4 suspension at 353 K with vigorously stirring for 1 h. Then, 5.58 ml of TEOS was rapidly added to the mixture, and the reaction was continued for another 2 h to form a blown colloidal suspension. The obtained brown colloidal nanoparticles were separated with a magnet, washed with ethanol for several times, and dried in vacuum at 60 °C for 24 h. Finally, the dried colloidal nanoparticles were calcined at 540 °C for 7 h to remove the surfactant CTAT and obtained MMS nanoparticles.

2.3 Synthesis of aminated MMS (MMS-NH₂) nanoparticles

MMS-NH₂ nanoparticles were obtained by a reaction between MMS and 3-aminopropyltriethoxysilane (APTES) in ethanol. Briefly, 300 mg of MMS nanoparticles was homogeneously dispersed in 60 ml of ethanol by ultrasonication. And then, 0.9 ml of APTES was added to the suspension and slowly stirred the suspension for 24 h at the room temperature. The mixture was collected by centrifugation and extensively washed with ethanol, and the obtained white particles dried in vacuum at 60 °C for 24 h.

2.4 Characterization

Scanning electron microscopy (SEM) was carried out with an FEI Quanta 450 field emission scanning electron microscope. Transmission electron microscopy (TEM) images were obtained using a JEM-2100F transmission electron microscope at an acceleration voltage of 200 kV. The wide angle X-ray diffraction (WAXRD) patterns were obtained on a D8 ADVANCE powder diffractometer using Cu K α 1 radiation (1.5405 Å). Dynamic light scattering (DLS) measurements were performed on a

Malvern zeta sizer Nano-ZS90. N₂ adsorption-desorption isotherms were obtained on a Micromeritics Tristar 3020 automated surface area and pore size analyzer at 77 K under continuous adsorption conditions. Brunauer-Emmett-Teller (BET) and Barrett-Joyner-Halenda (BJH) methods were used to determine the surface area and pore size distribution. Magnetization curves were carried out using a TF-WI-ZDYP V 3.0.4 vibrating sample magnetometer (VSM) at 298 K. UV-Vis absorption spectra were measured on a NanoDrop 2000C spectrophotometer.

2.5 Binding of CpG ODN to MMS-NH₂ nanoparticles (CpG/MMS-NH₂ complexes)

The sequence of CpG ODN molecule was 5'-TCAGAGAGTTAGAGAGTTAGAGAGTCAGAGAGTTAGAGAGTTAGAGAGTTAGAGAGTTAGAGAGTTAGAGAGTTAGAGAG-3' (72 bases), and CpG ODN was dissolved in ultrapure water at a concentration of 1 µg/µl and stored at -20 °C until use.

To study electrostatic binding of CpG ODN to MMS-NH₂ nanoparticles, MMS-NH₂ nanoparticles were suspended in ultrapure water with a concentration of 1 µg/µl. Subsequently, the as-prepared MMS-NH₂ suspension was dispersed in CpG ODN solution and the mixture with a weight ratio of MMS-NH₂/CpG ODN = 5, 10, 20, 50 and 100 was shaken at room temperature for 4 h, respectively. The mixture was centrifuged at 12,000 rpm for 15 min to collect the CpG/MMS-NH₂ complexes. The supernatant was collected for UV-vis analysis to estimate the adsorbed amount of CpG ODN. The remained supernatants were analyzed with gel electrophoresis by loading onto 3% agarose gel with ethidium bromide and running with loading buffer at 120 V for 20 min.

2.6 Stability of CpG/MMS-NH₂ complexes in FBS solution

200 µg of CpG/MMS-NH₂ complexes containing 3 µg of CpG ODN was incubated in an aqueous solution of 25% FBS at 37 °C for 0, 2, 5 and 8 h, respectively. As a control, 3 µg of free CpG ODN was also treated in 25% FBS solution at 37 °C for 0, 2, 5 and 8 h, respectively. After digestion, 2 µl of 250 mM EDTA was respectively added to all samples, and treated for 2 min at 80 °C to quench the digestion reaction. Then, the FBS-treated CpG/MMS-NH₂ complexes were dispersed in aqueous solution for CpG ODN releasing under ultrasonication. After releasing for 5 h, the samples were centrifugated at 12,000 rpm for 15 min to separate the CpG/MMS-NH₂ complexes, and supernatants were then analyzed with gel electrophoresis by loading onto 3% agarose gel with ethidium bromide and running with loading buffer at 120 V for 20 min. The FBS-treated free CpG ODN were also analyzed with gel electrophoresis as same as above procedures.

2.7 Cell culture

Raw 264.7 cells stably expressing TLR9 were purchased from RIKEN (Japan), and grown in Minimum essential medium (MEM, GIBCO) supplemented with 10% FBS, 100 U/ml penicillin, 100 µg/ml streptomycin, and 0.1 mM non-essential amino acid at 37 °C in humidified air containing 5 % CO₂. Raw 264.7 cells were cultured according to manufacture instructions.

2.8 In vitro cytotoxicity assay

An in vitro cytotoxicity assay for MMS-NH₂ nanoparticles was performed using a Cell Counting Kit-8 (CCK-8, Dojindo, Japan). Raw 264.7 cells were seeded in a 96-well

plate at a density of 5000 cells/well. After seeding cells for 24 h, MMS-NH₂ nanoparticles solution (1 mg/ml in MEM) was added in 96-well plate. The final concentrations of MMS-NH₂ nanoparticles were 0, 25, 50, 75, 100 and 200 µg/ml, and the final medium volume in each well was 100 µl. After incubation of cells for 24 h, 10 µl of CCK-8 solution was added in each well, and the cells were incubated for another 3 h. Absorbance at 450 nm was then measured using a microplate reader (MTP-880 Lab, Corona, Japan). Cytotoxicity was expressed as the percentage of viable cells compared with that of untreated control cells.

2.9 Cellular uptake assay

To investigate cellular uptake of CpG/MMS-NH₂ complexes, fluorescein isothiocyanate (FITC)-labeled CpG ODN (FITC-CpG ODN) were loaded on MMS-NH₂ nanoparticles. Raw 247.6 cells were seeded in a 35 mm glass bottom Petri dish at a density of 1.5×10^4 cells/cm². After incubation of cells for 24 h, FITC-CpG/MMS-NH₂ complexes were added in the dish at a final concentration of 100 µg/ml. When the cells had been incubated for another 15 h, the culture medium was removed, and the cells were washed with PBS twice. Subsequently, the cells were fixed with 4% paraformaldehyde for 15 min, and washed with PBS twice. Then, the cells were permeabilized with 0.2% Tween-20 at room temperature for 10 min and preincubated in 1% BSA/PBS for 1 h. Finally, the cells were stained with LAMP1 antibody (ab24170, Abcam) at room temperature for 1h, washed with PBS twice, and then stained with Alexa Fluor 555 goat anti-rabbit IgG (A21428, Invitrogen) at room temperature for 1 h. The cells were washed with PBS twice and visualized using a

confocal laser scanning microscope (CLSM, SP5, Leica), and the excitation laser wavelengths for FITC and Alexa Fluor 555 were 488 and 543 nm, respectively.

2.10 Cytokine assay

Raw 264.7 cells were seeded in a 96-well plate at a density of 1×10^5 cells/well in MEM medium. After incubation of cells for 24 h, the cells were stimulated with CpG/MMS-NH₂ complexes (CpG ODN concentration: 5 µg/ml). For the controls, free CpG ODN, MEM medium and MMS-NH₂ nanoparticles without CpG ODN were added in the culture medium at equal concentrations of CpG ODN and MMS-NH₂ nanoparticles. After 15 h of incubation at 37 °C, the cells were washed with PBS twice, and total RNA was extracted using Isogen solution (Wako, Japan) and treated with a DNase I digestion step according to the manufacture's instructions. The obtained RNA was reverse transcribed into complementary DNA (cDNA) using a primeScript™ RT reagent Kit (Takara, Japan). The cDNA was analyzed for marker of interleukin-6 (IL-6). Glyceraldehyde 3-phosphate dehydrogenase (Gapdh) was utilized as a reference. RT-PCR was performed using LightCycler FastStart DNA Master SYBER Green I Kit (Roche Appl. Sci. Japan). Relative expression level for IL-6 was normalized against the initial concentration value of the reference gene Gapdh and determined by using the second derivative maximum method.

3. Results and discussion

3.1 Synthesis of MMS and MMS-NH₂ nanoparticles

Fig. 2A shows wide-angle XRD pattern of MMS nanoparticles. A broad reflection

at $2\theta=20-25^\circ$ suggested the amorphous structure of mesoporous silica matrix, and other well-resolved diffraction peaks were attributed to Fe_3O_4 nanoparticles according to the reflection peak positions and relative intensities. The results indicated that the embedded Fe_3O_4 nanoparticles maintained their crystalline structure after the encapsulation in mesoporous silica matrix. Fig. 2B shows the magnetization curve of MMS nanoparticles measured at 298 K. Very small hysteresis loop was detected for MMS nanoparticles, and the coercivity and the remanence were 3.5 Oe and 0.3 emu/g, respectively, indicating the superparamagnetic behavior of MMS nanoparticles. The saturation magnetization value of MMS nanoparticles was estimated to be 6.5 emg/g, so that MMS nanoparticles can respond to the external magnetic field quickly.

Fig. 3 shows TEM images of MMS nanoparticles. It can be observed that MMS nanoparticles were spherical and highly monodisperse. Most of MMS nanoparticles were evenly uniform in particle size, and the average particle size was estimated to be 150 nm. Concurrently, the DLS study demonstrated that a hydrodynamic particle size of MMS nanoparticles was ca. 190 nm (Fig. 4A), which is larger than the particle size observed by TEM. It might be that DLS measures the hydrodynamic diameter of the particles including the solvation layers. Importantly, a low polydispersity index (PDI) of 0.044 obtained from DLS measurement indicates the stability and a narrow particle size distribution of MMS nanoparticles in solution. On the other hand, from TEM images, one to several Fe_3O_4 nanoparticles were embedded in each MMS nanoparticle, and the branched mesopores could be observed on MMS

nanoparticles.

N_2 adsorption-desorption isotherm of MMS nanoparticles together with the corresponding pore size distribution are shown in Fig. 5. The isotherm can be classified as type IV isotherm, demonstrating the mesoporous characteristics of MMS nanoparticles. The BET surface area (S_{BET}) and single point adsorption pore volume (V_P) at $P/P_0=0.97$ for MMS nanoparticles were $462.4 \text{ m}^2/\text{g}$ and $0.623 \text{ cm}^3/\text{g}$, respectively. Furthermore, the corresponding pore size distribution of MMS nanoparticles exhibited a bimodal mesopore size distribution peaked at 3.4 and 10.7 nm, which might be resulted from the CTAT templating surfactant and TEA mineralizing agent. Therefore, from the viewpoint of structure, the reasonable particle size together with the large and branched mesoporous structure could make such MMS nanoparticles suitable to be used as gene carriers.

For binding CpG ODN to MMS nanoparticles, MMS nanoparticles were modified with amino groups to obtain positively charged surface, which facilitate the binding of negatively charged CpG ODN to MMS nanoparticles through electrostatic interaction. Zeta potentials of MMS and MMS-NH₂ nanoparticles are shown in Fig. 6. It can be observed that zeta potential of MMS nanoparticles was $-14.88 \pm 0.19 \text{ mV}$, while that of the MMS-NH₂ nanoparticles was $6.09 \pm 0.25 \text{ mV}$ due to the modification of positively charged amino groups onto MMS nanoparticles. On the other hand, N_2 physisorption measurement showed that the BET surface area of MMS-NH₂ nanoparticles decreased to be $315.2 \text{ m}^2/\text{g}$ due to the grafting of amino groups on the mesopore surface, and the bimodal mesopore size distribution also exhibited a slight

decrease to be peaked at 3.2 and 10.6 nm (Fig. 5). The amino modification of MMS nanoparticles induced a slight increase in the hydrodynamic particle size (ca. 220 nm), but the low PDI of 0.159 indicated that MMS-NH₂ nanoparticles maintained the narrow particle size distribution and good dispersity (Fig. 4B).

3.2 Preparation and serum stability of CpG/MMS-NH₂ complexes

In generally, binding of DNA onto nanoparticles could efficiently protect DNA from degradation by nucleases, because the microenvironment of DNA molecules is changed to hinder enzymes to interact with the active sites of DNA molecules [51]. In this study, CpG ODN was bonded to MMS-NH₂ nanoparticles through electrostatic interaction to form the CpG/MMS-NH₂ complexes. Zeta potential decreased from 6.09 ± 0.25 mV to -5.85 ± 0.34 mV after binding of CpG ODN onto MMS-NH₂ nanoparticles (Fig. 6), and a little increase in hydrodynamic particle size (ca. 262 nm, PDI=0.211) after binding of CpG ODN on MMS-NH₂ nanoparticles (Fig. 4C), confirming that CpG ODN have bonded to MMS-NH₂ nanoparticles. Fig. 7 shows the CpG ODN loading capacity on MMS-NH₂ nanoparticles at different weight ratio of MMS-NH₂ nanoparticles to CpG ODN. It can be observed that the saturation loading of CpG ODN on MMS-NH₂ nanoparticles was at a weight ratio of ≤ 10 . Determining by UV-vis analysis, the loading capacity of CpG ODN on MMS-NH₂ nanoparticles at a weight ratio of 5 was estimated to be 41.4 ± 0.5 $\mu\text{g}/\text{mg}$, which was much higher than those on chitosan-coated BN nanospheres (27.2 $\mu\text{g}/\text{mg}$) and PLL-functionalized magnetic silica spheres (22.5 $\mu\text{g}/\text{mg}$) [39,48]. Therefore, MMS-NH₂ nanoparticles as

carriers can bind CpG ODN with high loading capacity, and may enhance the stability of CpG ODN.

Serum stability of free CpG ODN and CpG/MMS-NH₂ complexes was tested in 25% serum-containing medium using gel electrophoresis. As shown in Fig. 8A, the band of free CpG ODN became weaker with increasing the treatment time, and completely disappeared after 8 h digestion, suggesting that free CpG ODN was gradually degraded in serum-containing medium. While for CpG/MMS-NH₂ complexes (Fig. 8B), the bands of the released CpG ODN exhibited a little weaker after digestion, but they were clearly observed even after 8 h digestion, which indicated that CpG/MMS-NH₂ complexes enhanced the stability to protect CpG ODN against degradation by nucleases. Therefore, binding of CpG ODN onto MMS-NH₂ nanoparticles enhanced the serum stability of CpG ODN, which would be useful for stimulating the induction of cytokines, and thereby enhancing immune response.

3.3 In vitro cytotoxicity, cellular uptake and IL-6 induction of CpG/MMS-NH₂ complexes

Investigation of the cytotoxicity of drug/DNA delivery vehicles is necessary for drug/gene delivery. In this study, in vitro cytotoxicity of MMS-NH₂ nanoparticles to Raw 264.7 cells was evaluated using Cell Counting Kit-8 (CCK-8) assay. As shown in Fig. 9, after incubation of cells with MMS-NH₂ nanoparticles for 24 h, no cytotoxicity was observed even at a concentration of 200 µg/ml, which suggest that MMS-NH₂ nanoparticles are safe and could be used as nonviral carrier for CpG ODN delivery.

The evidence indicates that intracellular CpG ODN delivery is necessary to initiate the TLR9-mediated induction of multiple cytokines and chemokines, and thereby modulates the immune response, because the activation of TLR9 by CpG ODN occurs in the endosome or endolysosome [52]. Therefore, cellular uptake of CpG/MMS-NH₂ complexes was investigated in this study. Fluorescein isothiocyanate (FITC)-labeled CpG ODN was loaded onto MMS-NH₂ nanoparticles to form FITC-CpG/MMS-NH₂ complexes. The complexes were incubated with Raw 264.7 cells for 15 h and stained with LAMP1 to observe the intracellular localization of the FITC-CpG/MMS-NH₂ complexes using CLSM. Here, LAMP1 was chosen to identify the endolysosome vesicles in Raw 264.7 cells. As shown in Fig. 10, we observed that FITC-CpG/MMS-NH₂ complexes were localized in LAMP1-positive endolysosome, which suggest that MMS-NH₂ nanoparticles were not easy to escape from endosome to cytosol, and could be the efficient carriers for intracellular delivery of CpG ODN. Generally, nanoparticles are taken up into cells by endocytosis. The endocytosed vesicles that contain nanoparticles are fused with endosome. After fusion, this endosome that contains nanoparticles is further fused with lysosome, and the fused organelle is called endolysosome. TLR9 is localized in endosome and endolysosome. Therefore, binding of CpG ODN on MMS-NH₂ nanoparticles could efficiently internalize into cells and locate in the endolysosome, which promote the interaction of CpG ODN with TLR9, and thereby lead to cytokines induction and immune response.

To investigate the induction of cytokines by CpG/MMS-NH₂ complexes, IL-6

induction was evaluated using CpG/MMS-NH₂ complexes with a CpG ODN concentration of 5 µg/ml in culture medium to stimulate Raw 264.7 cells for 15 h. For comparison, the cells were also stimulated by free CpG ODN and MMS-NH₂ nanoparticles with the same CpG ODN or MMS-NH₂ amounts. As shown in Fig. 11, MEM medium and MMS-NH₂ nanoparticles did not stimulate IL-6 induction, suggesting that the culture medium and carriers can not simulate cytokine induction. Free CpG ODN induced lower level of IL-6 production (IL-6/Gapdh= 0.836±0.248), which might be attributed to the poor stability of free CpG ODN in culture medium. However, CpG/MMS-NH₂ complexes exhibited excellent ability to stimulate IL-6 induction and the IL-6 induction was estimated to be 1.551±0.041 for IL-6/Gapdh, which significantly enhanced the IL-6 induction compared to free CpG ODN. The results indicated that MMS-NH₂ nanoparticles could be used as carrier for CpG ODN delivery to simulate the TLR9-mediated immune response, which might be attributed to the high loading capacity, efficient cellular uptake and localization in endolysosome of CpG ODN delivery system using MMS-NH₂ nanoparticles. Therefore, MMS nanoparticles as carriers for delivering CpG ODN would significantly enhance the TLR9-mediated cytokine induction, and thereby promote immune responses.

4. Conclusion

In this study, a potential MMS nanoparticles-based CpG ODN delivery system has been developed by binding of CpG ODN onto aminated MMS nanoparticles with small particle size and large mesopore size. MMS nanoparticles exhibited

superparamagnetic behavior with saturation magnetization of 6.5 emu/g, and had a high CpG ODN loading capacity (ca. 41.4 $\mu\text{g}/\text{mg}$) due to the contribution of high surface area and large mesopore channels. In vitro cytotoxicity assay showed that MMS-NH₂ nanoparticles had no cytotoxicity to Raw 264.7 cells. Compared to free CpG ODN, CpG/MMS-NH₂ complexes enhanced serum stability for protecting CpG ODN against degradation. Most importantly, CpG/MMS-NH₂ complexes could retain in the endolysosome after endocytosis by cells, and significantly induced higher level of IL-6 production compared to free CpG ODN. Therefore, MMS nanoparticles as carriers for delivering CpG ODN could be targeting and significantly enhance the TLR9-mediated cytokine induction, and thereby promote immune responses.

Acknowledgements

The authors gratefully acknowledge the support by the Program for Professor of Special Appointment (Eastern Scholar) at Shanghai Institutions of Higher Learning, National Natural Science Foundation of China (No. 51102166), Shanghai Shuguang Project (No. 12SG39), Program for New Century Excellent Talent in University (No. NCET-12-1053), Key Project of Chinese Ministry of Education (No. 212055), Innovation Program of Shanghai Municipal Education Commission (No. 12ZZ140), the Huijiang Foundation of China (No. B14006) and Training Program of University of Shanghai for Science and Technology (No. 14XPY01).

References:

[1] I. M. Verma, N. Somia, *Nature* 1997, **389**, 239-242.

- [2] I. M. Verma, M. D. Weitzman, *Annu. Rev. Biochem.* 2005, **74**, 711-738.
- [3] T. Zhang, *Current Drug Delivery* 2014, **11**, 233-242.
- [4] F. Touzot, S. Hacein-Bey-Abina, A. Fischer, M. Cavazzana, *Expert Opinion on Biological Therapy* 2014, **14**, 789-798.
- [5] J. M. Wilson, *Human Gene Therapy* 2014, **25**, 257-261.
- [6] M. A. Kay, J. C. Glorioso, L. Naldini, *Nature Med.* 2001, **7**, 33-40.
- [7] S. D. Li, L. Huang, *Gene Therapy* 2006, **13**, 1313-1319.
- [8] I. I. Slowing, J. L. Vivero-Escoto, C. W. Wu, V. S. Y. Lin, *Adv. Drug Deliv. Rev.* 2008, **60**, 1278-1288.
- [9] Q. J. He, J. L. Shi. *J. Mater. Chem.* 2011, **21**, 5845-5855.
- [10] C. Hom, J. Lu, F. Tamanoi, *J. Mater. Chem.* 2009, **19**, 6308-6316.
- [11] X. Du, B. Shi, Y. Tang, S. Dai, S. Z. Qiao, *Biomaterials* 2014, **35**, 5580-5590.
- [12] T. Xia, M. Kovichich, M. Liong, H. Meng, S. Kabehie, S. George, J. I. Zink, A. E. Nel, *ACS Nano* 2009, **3**, 3273-3286.
- [13] M. H. Kim, H. K. Na, Y. K. Kim, S. R. Ryoo, H. S. Cho, K. E. Lee, *ACS Nano* 2011, **5**, 3568-7356.
- [14] F. Gao, P. Botella, A. Corma, J. Blesa, L. Dong. *J. Phys. Chem. B* 2009, **113**, 1796-1804.
- [15] H. K. Na, M. H. Kim, K. Park, S. R. Ryoo, K. E. Lee, H. Jeon, R. Ryoo, C. Hyeon, D. H. Min, *Small* 2012, **8**, 1752-1761.
- [16] S. B. Hartono, W. Gu, F. Kleitz, J. Liu, L. He, A. P. J. Middelberg, C. Yu, G. Q. Lu, S. Z. Qiao, *ACS Nano* 2012, **6**, 2104-2117.

- [17] D. R. Radu, C. Y. Lai, K. Jeftinija, E. W. Rowe, S. Jeftinija, V. S. Y. Lin. *J. Am. Chem. Soc.* 2004, **126**, 13216-13217.
- [18] X. Ma, K. T. Nguyen, P. Borah, C. Y. Ang, Y. Zhao. *Adv. Health Mater.* 2012, **1**, 690-697.
- [19] D. Lin, Q. Cheng, Q. Jiang, Y. Huang, Z. Yang, S. Han, Y. Zhao, S. Guo, Z. Liang, A. Dong. *Nanoscale* 2013, **5**, 4291-4301.
- [20] S. B. Hartono, N. T. Phuoc, M. Yu, Z. Jia, M. J. Monteiro, S. Z. Qiao, C Yu. *J. Mater. Chem. B* 2014, **2**, 718-726.
- [21] T.-Y. Kim, M. Kim, M. Eltohamy, Y.-R. Yun, J.-H. Jang, H. W. Kim. *J. Biomed. Mater. Res. Part A* 2013, **101**, 1651-1660.
- [22] I. Y. Park, I. Y. Kim, M. K. Yoo, Y. J. Choi, M.-H. Cho, C. S. Cho. *Int. J. Pharm.* 2008, **359**, 280–287.
- [23] F. Torney, B. G. Trewyn, V. S.-Y. Lin, K. Wang, *Nature Nanotechnol.* 2007, **2**, 295–300.
- [24] A. M. Chen, M. Zhang, D. Wei, D. Stueber, O. Taratula, T. Minko, H. He, *Small* 2009, **5**, 2673–2677.
- [25] F. Qin, Y. Zhou, J. Shi, Y. Zhang, *J. Biomed. Mater. Res.* 2009, **90A**, 333–338.
- [26] C. Tao, Y. Zhu, Y. Xu, M. Zhu, H. Morita, N. Hanagata, *Dalton Trans.* 2014, **43**, 5142-5150.
- [27] M. Wang, X. Li, Y. Ma, H. Gu, *Int. J. Pharm.* 2013, **448**, 51-57.
- [28] Q. Gan, D. W. Dai, Y. Yuan, J. C. Qian, S. Sha, J. L. Shi, C. S. Liu, *Biomedical Microdevices*, 2012, **14**, 259-270.

- [29] M. P. Dobay, A. Schmidt, E. Mendoza, T. Bein, J. O. Radler, *Nano. Lett.* 2013, **13**, 1047-1052.
- [30] J. Tu, T. X. Wang, W. Shi, G. S. Wu, X. H. Tian, Y. H. Wang, D. T. Ge, L. Ren, *Biomaterials*, 2012, **33**, 7903-7914.
- [31] A. M. Sauer, A. Schlossbauer, N. Ruthardt, V. Cauda, T. Bein, C. Brauchle, *Nano. Lett.* 2010, **10**, 3684-3691.
- [32] B. Jahrsdörfer, G. J. Weiner, *Curr. Opin Investig Drugs* 2003, **4**, 686–690.
- [33] D. E. Fonseca, J. N. Kline. *Adv. Drug Deliv. Rev.* 2009, **61**, 256–262.
- [34] D. M. Klinman, S. Klaschik, T. Sato, D. Tross. *Adv. Drug Deliv. Rev.* 2009, **61**, 248–255.
- [35] N. Hanagata, *Inter. J. Nanomed.* 2012, **7**, 2181-2195.
- [36] A. M. Krieg, A. K. Yi, S. Matson, T. J. Waldschmidt, G. A. Bishop, R. Teasdale, G. A. Koretzky, D. M. Klinman, *Nature*, 1995, **374**, 546-549.
- [37] N. L. Bernasconi, E. Traggiai, A. Lanzavecchia, *Science* 2002, **298**, 2199-2202.
- [38] V. Sokolova, T. Knuschke, A. Kovtun, J. Buer, M. Epple, A. M. Westendorf, *Biomaterials*. 2010, **31**, 5627–5633.
- [39] H. J. Zhang, S. Chen, C. Y. Zhi, T. Yamazaki, N. Hanagata, *Inter. J. Nanomed.* 2013, **8**, 1783-1793.
- [40] S. Chen, H. J. Zhang, S. Chinnathambi, N. Hanagata, *Mater. Sci. Eng. C*, 2013, **33**, 3382-3388.
- [41] Y. F. Zhu, W. J. Meng, X. L. Li, H. Gao, N. Hanagata, *J. Phys. Chem. C*. 2010, **115**, 447–452.

- [42] H. C. Chen, B. Sun, K. K. Tran, H. Shen. *Biomaterials* 2011, **32**, 1731-1737.
- [43] I. Gursel, M. Gursel, K. J. Ishii, D. M. Klinman. *J. Immunol.* 2001, **167**, 3324-3328.
- [44] C. Sun, J. S. H. Lee, M. Zhang. *Adv. Drug Deliv. Rev.* 2008, **60**, 1252-1265.
- [45] W. R. Zhao, J. L. Gu, L. X. Zhang, H. R. Chen, J. L. Shi. *J. Am. Chem. Soc.* 2005, **127**, 8916-8917.
- [46] J. Kim, H. S. Kim, N. Lee, T. Kim, H. Kim, T. Yu, I. C. Song, W. K. Moon, T. Hyeon, *Angew. Chem. Int. Ed.* 2008, **47**, 8438-8441.
- [47] J. Dobson, *Gene Therapy* 2006, **13**, 283-287
- [48] J. Liu, B. Wang, S. B. Hartono, T. Liu, P. Kantharidis. *Biomaterials* 2012, **33**, 970-978.
- [49] J. Zhang, W. Sun, L. Bergman, J. M. Rosenholm, M. Linden, G. Wu, H. Xu, H. C. Gu. *Mater. Lett.* 2012, **67**, 379-382.
- [50] Y. S. kang, S. Risbud, J. F. Rabolt. *Chem. Mater.* 1996, **8**, 2209-2211.
- [51] M. Malmsten, *Current Opinion Colloid Interface Sci.* 2013, **18**, 468-480.
- [52] G. K. Mutwiri, A. K. Nichani, S. Baniuk, L. A. Baniuk. *J. Controlled Release* 2004, **97**, 1-17.

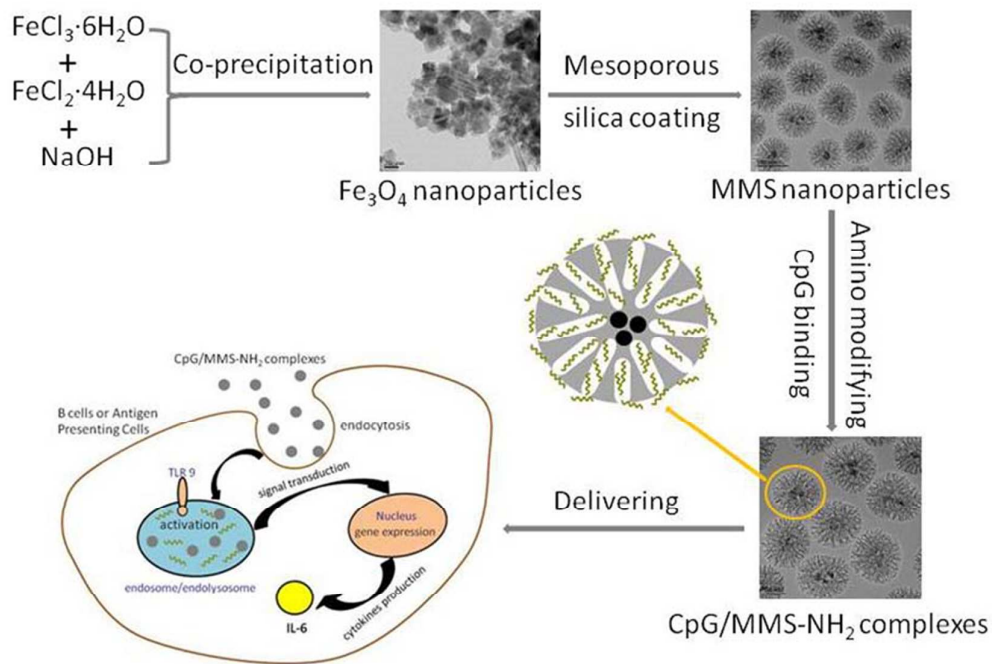


Fig. 1 schematic drawing for the preparation of MMS nanoparticles-based CpG ODN delivery system.

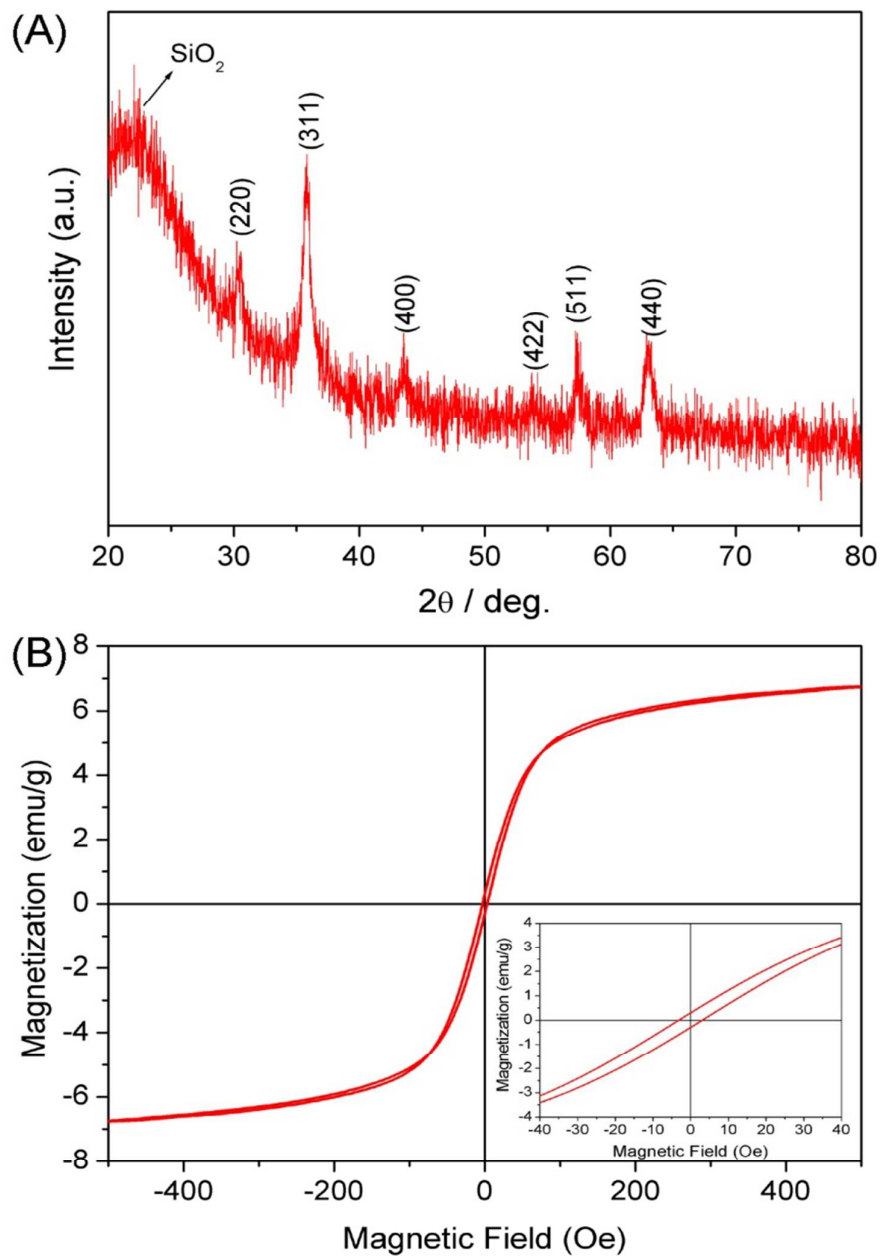


Fig. 2 (A) Wide angle XRD patterns of MMS nanoparticles; (B) Magnetization curve of

MMS nanoparticles measured at 298 K.

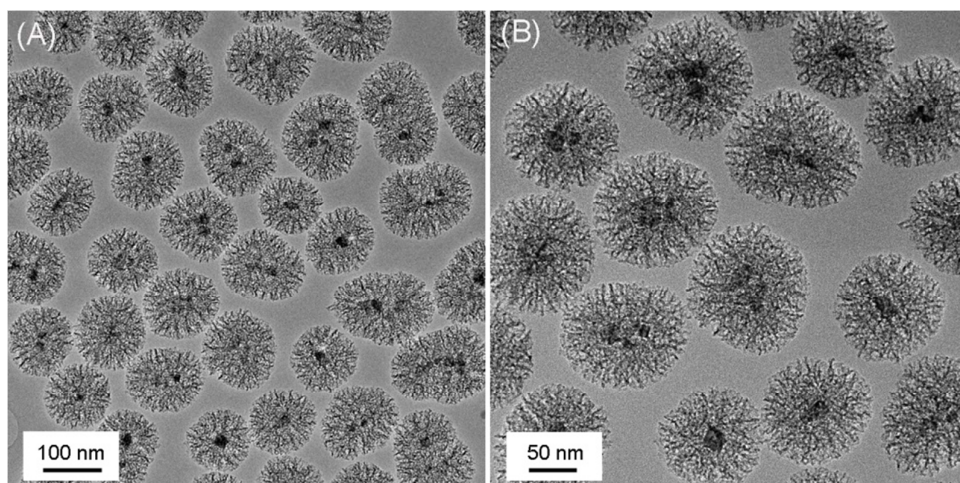


Fig. 3 TEM image of MMS nanoparticles.

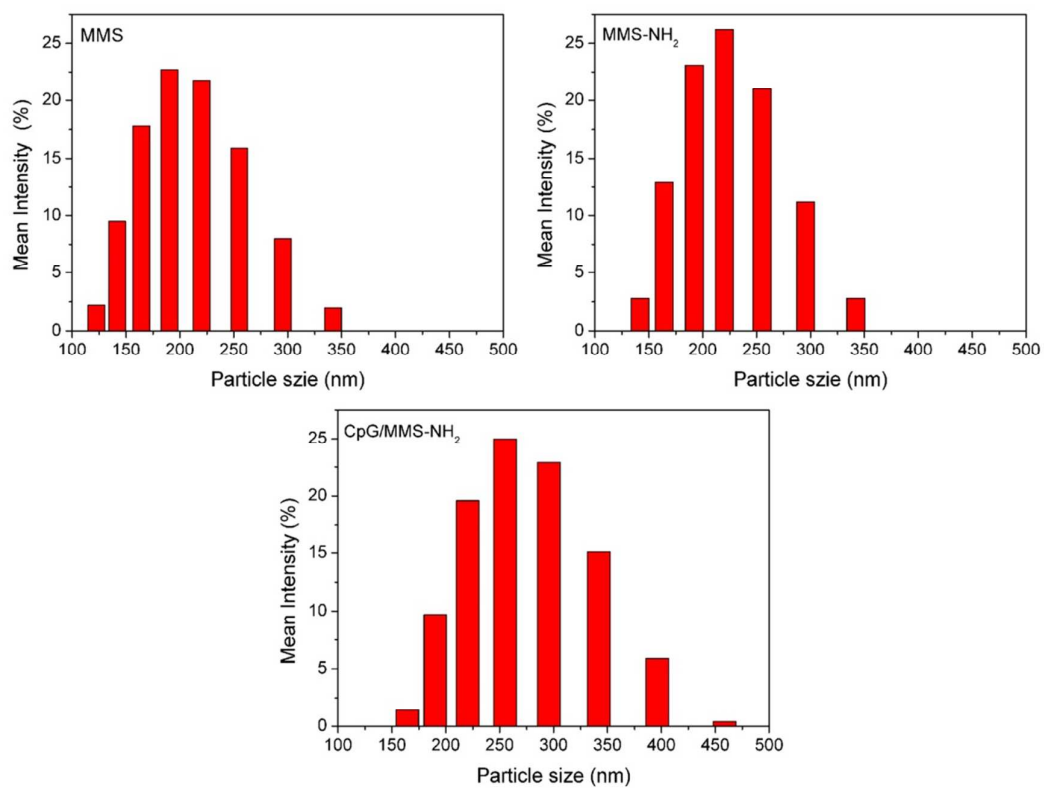


Fig. 4 Particle size distributions of the MMS, MMS-NH₂ nanoparticles and CpG/MMS-NH₂ complexes in H₂O, as measured by dynamic light scattering (DLS).

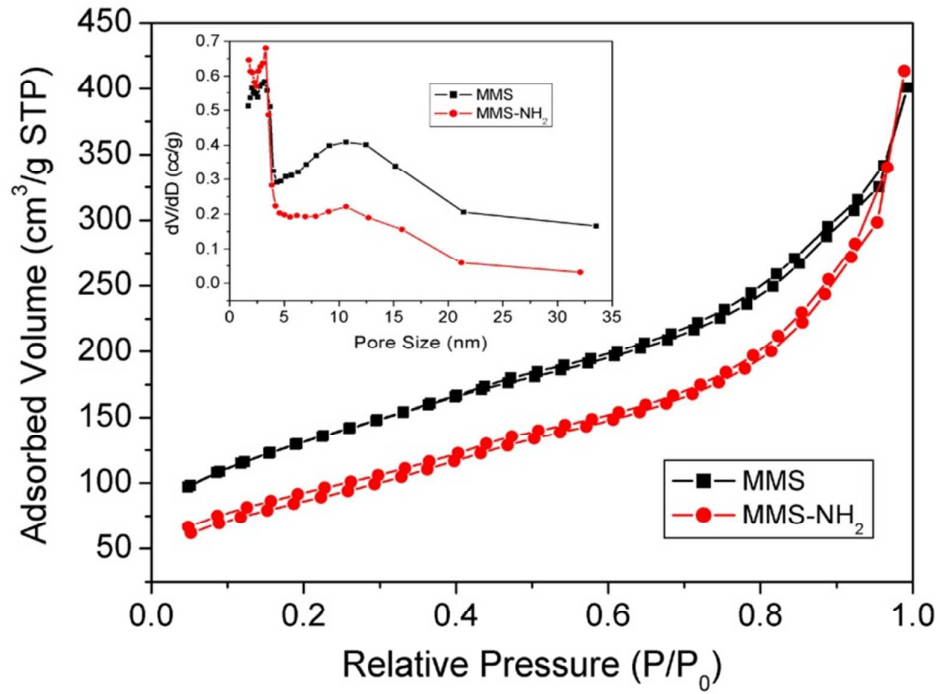


Fig. 5 N₂ adsorption-desorption isotherms and the corresponding pore size distributions of the MMS and MMS-NH₂ nanoparticles.

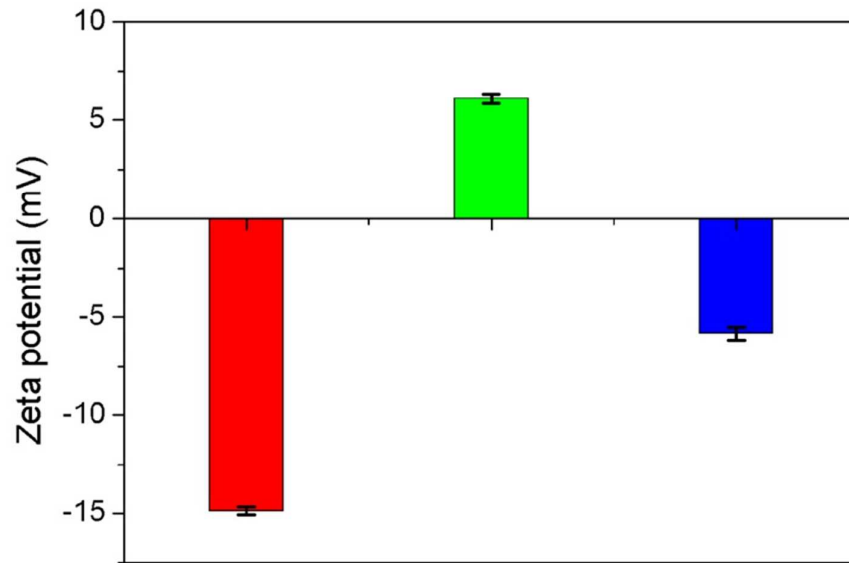


Fig. 6 Zeta potentials of the MSNs, MMS-NH₂ nanoparticles and CpG/MMS-NH₂ complexes in PBS.

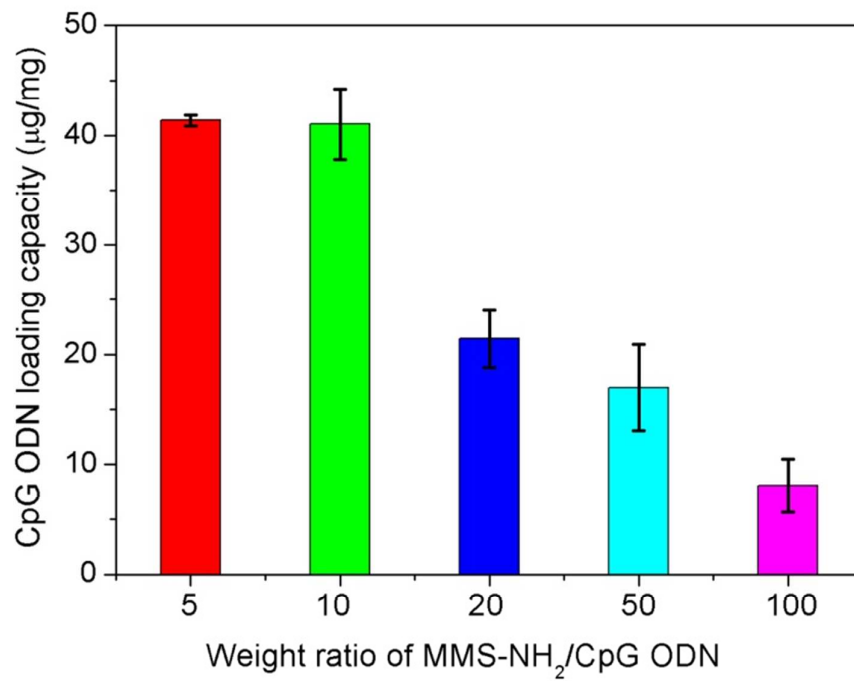


Fig. 7 CpG ODN loading capacities on MMS-NH₂ nanoparticles at various weight ratios of MMS-NH₂ nanoparticles to CpG ODN.

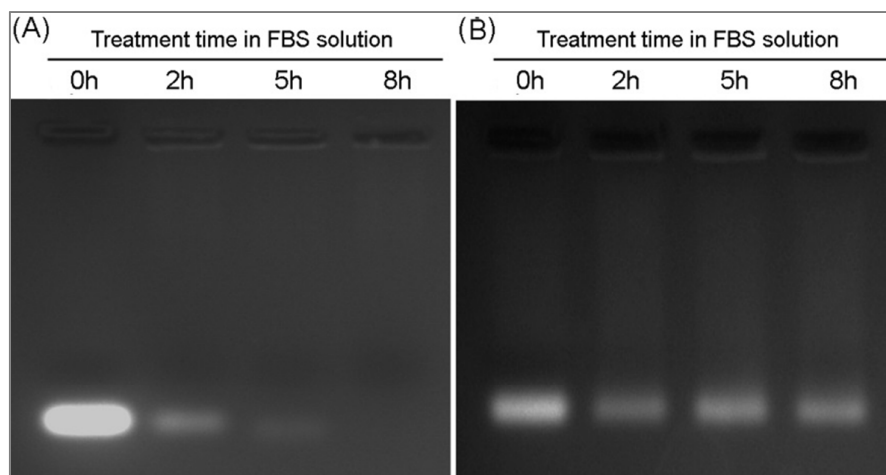


Fig. 8 Serum stability of (A) free CpG ODN and (B) CpG/MMS-NH₂ complexes in 25% serum-containing media, as measured by agarose gel electrophoresis.

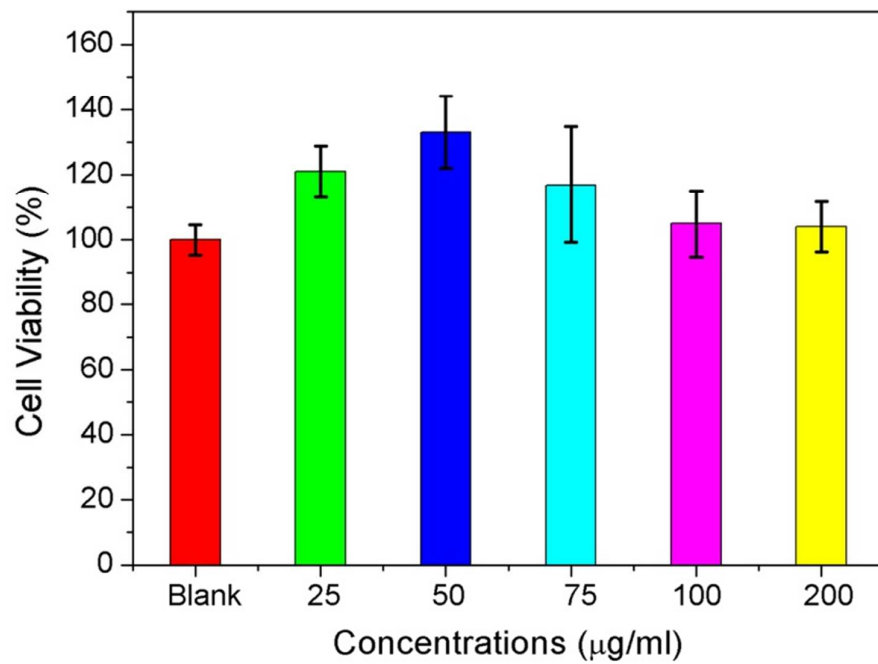


Fig. 9 Effect of the concentrations of MMS-NH₂ nanoparticles on the cytotoxicity to Raw 264.7 cells, as measured by a Cell Counting Kit-8 assay.

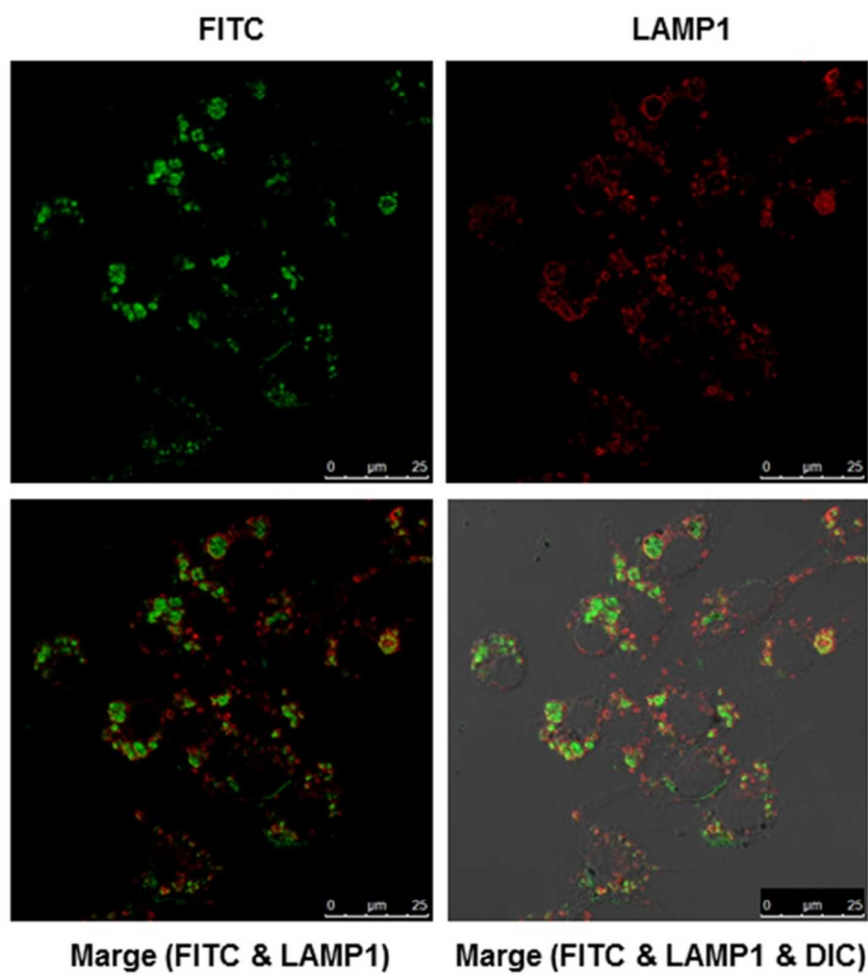


Fig. 10 Cellular uptake and intracellular localization of CpG/MMS-NH₂ complexes after 15 h of incubation with a concentration of 100 μg/ml. Green: CpG/MMS-NH₂ complexes; Red: endolysosomal membranes.

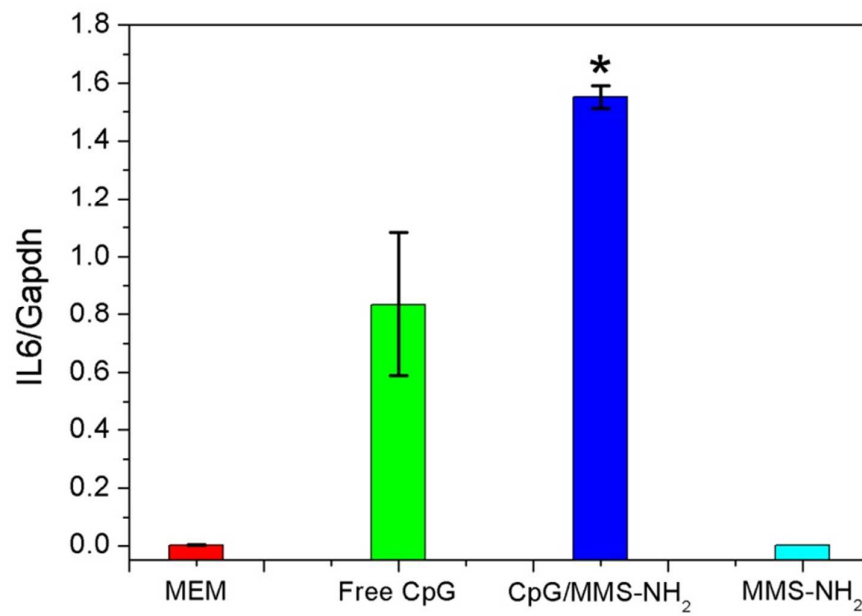


Fig. 11 IL-6 induction by Raw 264.7 cells cultured with MEM, MSN-NH₂ nanoparticles, free CpG ODN and CpG/MSN-NH₂ complexes (* P<0.05).